Journal of *Marine Science and Engineering*

MDPI

Article

Numerical Study on the Expansion and Variation of Changjiang Diluted Water in Summer and Autumn

Wanli Hou [1], Menglin Ba [1], Jie Bai [2] and Jianghua Yu [1,*]

[1] Jiangsu Key Laboratory of Atmospheric Environment Monitoring and Pollution Control, School of Environmental Science and Engineering, Nanjing University of Information Science & Technology, Nanjing 210044, China; 20181213006@nuist.edu.cn (W.H.); 20191213002@nuist.edu.cn (M.B.)

[2] Key Laboratory of Marine Environment and Ecology, College of Environmental Science and Engineering, Ocean University of China, Ministry of Education, Qingdao 266100, China; baijie@ouc.edu.cn

* Correspondence: yujh@nuist.edu.cn; Tel.: +86-25-58695677; Fax: +86-25-58731090

Abstract: In view of the expansion and directional change mechanisms of Yangtze River water diluted with sea water in the shelf region (also known as Changjiang diluted water [CDW]) during summer and autumn, a three-dimensional hydrodynamic model of the Yangtze River Estuary (YRE) and its adjacent waters was established based on the Finite Volume Community Ocean Model (FVCOM). Compared with the measured data, the model accurately simulates the hydrodynamic characteristics of the YRE. On that basis, the influence of the expansion patterns of the CDW in both summer and autumn was studied. It was found that, in 2019, the CDW expanded to the northeast in the summer and to the southeast in the autumn, and that the route of the CDW is mainly controlled by the wind, not the runoff. Current seasonal winds also change the transportation route of the CDW by affecting its hydrodynamic field. Typhoons are frequent in both summer and autumn, causing abnormalities in both the transportation route and expansion of the CDW. During a typhoon, a large amount of the CDW is transported in a continuous and abnormal manner, accelerating the path turning of the CDW. This paper enhances the existing theoretical research of the CDW and provides a reference with respect to the expansion of diluted water all over the world.

Keywords: Finite Volume Community Ocean Model (FVCOM); Yangtze River Estuary (YRE); Changjiang diluted water (CDW); typhoon

check for updates

Citation: Hou, W.; Ba, M.; Bai, J.; Yu, J. Numerical Study on the Expansion and Variation of Changjiang Diluted Water in Summer and Autumn. *J. Mar. Sci. Eng.* **2021**, *9*, 317. https://doi.org/10.3390/jmse9030317

Received: 9 February 2021
Accepted: 6 March 2021
Published: 13 March 2021

Publisher's Note: MDPI stays neutral with regard to jurisdictional claims in published maps and institutional affiliations.

Copyright: © 2021 by the authors. Licensee MDPI, Basel, Switzerland. This article is an open access article distributed under the terms and conditions of the Creative Commons Attribution (CC BY) license (https://creativecommons.org/licenses/by/4.0/).

1. Introduction

Water that is mixed with sea water and the discharge of the Yangtze River (YR) in the shelf region is called Changjiang diluted water (CDW), and its horizontal expansion range varies with the seasons. Based on the records of the *Bulletin of China Marine Environmental Status*, about 70% of the nutrients discharged into the East China Sea were from the YR during the 2002–2017 period [1]. The CDW usually carries a large amount of nutrients and organic matter, contributing to higher levels of primary productivity, and has an important impact on the biogeochemical biology of the estuary. Because many marine biological and chemical activities are very sensitive to changes in nutrients and salinity [2,3], such changes affect the original stability and biodiversity of the marine ecosystem and can have many adverse effects on the development of coastal marine fisheries and the sustainable use of marine ecological resources. Study of the expansion and variation of the CDW is of great scientific significance to further research on marine ecology, and also provides a reference for other estuaries around the world, such as the Gulf of Mexico and Pamlico Sound, for example.

The characteristics of the CDW are entirely determined by specific environmental factors including the Kuroshio, baroclinic effects, the wind and the Taiwan warm current. These environmental factors are not only complex but also changeable; their effects are sometimes consistent, while at other times they counteract each other [4,5]. A considerable

body of research has been conducted to understand the expansion of the CDW by means of numerical simulation, theoretical methods and the analysis of measured data. According to the relationship observed between the position of the monthly average diluted water tongue and the runoff of the YR, Le [6] recorded a critical runoff which could influence the flow direction when the runoff exceeds the critical value. Other scholars have proposed that wind is a key factor affecting the path turning of the CDW, that the influence of runoff is limited and only affects its expansion range. The hydrodynamic environment of the East China Sea has been simulated over a long period of time and it was found that the expansion of the CDW to the northeast was mainly affected by the east wind or strong southeast winds, while the expansion area of the CDW near the estuary was mainly controlled by the runoff [7]. This finding was similar to the conclusions of Liu et al. [8], Wang et al. [9] and Zhou et al. [10]. Zhao [5] reported that the direct effect of wind may be circumstantial to the CDW, but the significant change of wind stress vorticity in winter and summer is one of the major reasons for altering the path of the CDW in both the flood and dry seasons. In addition, it is also believed that the Taiwan warm current is a leading factor for the path turning of the CDW [11–13]. Thus, there is no consensus on which factors dominate the transfer or expansion of the CDW. Moreover, while typhoons are one of the factors that affects the expansion of the CDW, there has been little research on the influence of typhoons on the expansion of the CDW. The aim of this study is to show the influence of the monsoon and typhoons on the variation and expansion of the CDW.

Considering the dispute on whether the expansion of the CDW is caused by runoff or the wind, the difference between the wind and runoff in summer and autumn is large. In addition, typhoon transit is often during summer and autumn and the impact on the CDW expansion needs to be explored. Therefore, this paper focuses on the variation of the CDW expansion in summer and autumn. Aiming to show the spreading morphology and seasonal variation of the CDW, the expansion variation and turning mechanism of the CDW under these multiple factors were studied by establishing a three-dimensional hydrodynamic model. The research in this paper enhances the theoretical research of the CDW and provides a reference with respect to the expansion of diluted water around the world.

2. Materials and Methods

2.1. Model Description

A three-dimensional numerical model, the Finite Volume Community Ocean Model (FVCOM), with unstructured triangular mesh and finite volume is used in this paper [14,15]. The unstructured triangular grid is used in the horizontal direction, which better fits the real coastline, while the sigma-coordinate is used to represent the irregular seabed topography in the vertical direction. The finite volume method, which combines the advantages of the finite element method and the finite difference method, is one of the most commonly used models for numerical solutions [16,17].

The main original equations of the FVCOM are as follows:

Continuity equation

$$\frac{\partial \zeta}{\partial t} + \frac{\partial Du}{\partial x} + \frac{\partial Dv}{\partial y} + \frac{\partial Dw}{\partial \sigma} = 0 \tag{1}$$

Momentum equation

$$\begin{aligned} &\tfrac{\partial uD}{\partial t} + u\tfrac{\partial uD}{\partial x} + v\tfrac{\partial uD}{\partial y} + w\tfrac{\partial u}{\partial \sigma} - fvD \\ &= -gD\tfrac{\partial \zeta}{\partial x} - \tfrac{gD}{\rho_0}[\tfrac{\partial}{\partial x}(D\int_{\sigma}^{0}\rho d\sigma^1) + \rho\sigma\tfrac{\partial D}{\partial x}] + \tfrac{1}{D}\tfrac{\partial}{\partial \sigma}(K_m\tfrac{\partial u}{\partial z}) + DF_x \end{aligned} \tag{2}$$

$$\begin{aligned} &\tfrac{\partial vD}{\partial t} + u\tfrac{\partial vD}{\partial x} + v\tfrac{\partial vD}{\partial y} + w\tfrac{\partial v}{\partial \sigma} - fuD \\ &= -gD\tfrac{\partial \zeta}{\partial y} - \tfrac{gD}{\rho_0}[\tfrac{\partial}{\partial y}(D\int_{\sigma}^{0}\rho d\sigma^1) + \rho\sigma\tfrac{\partial D}{\partial y}] + \tfrac{1}{D}\tfrac{\partial}{\partial \sigma}(K_m\tfrac{\partial v}{\partial z}) + DF_y \end{aligned} \tag{3}$$

Temperature, salinity and density equations

$$\frac{\partial TD}{\partial t} + u\frac{\partial TD}{\partial x} + v\frac{\partial TD}{\partial y} + w\frac{\partial T}{\partial \sigma} = \frac{\partial}{\partial \sigma}(K_h\frac{\partial T}{\partial \sigma}) + DF_T + D\hat{H} \quad (4)$$

$$\frac{\partial SD}{\partial t} + u\frac{\partial SD}{\partial x} + v\frac{\partial SD}{\partial y} + w\frac{\partial S}{\partial \sigma} = \frac{\partial}{\partial \sigma}(K_h\frac{\partial S}{\partial \sigma}) + DF_s \quad (5)$$

$$\rho = \rho(T, S) \quad (6)$$

where D is the total water depth; ζ is the free surface height; u, v and w are the velocity components of the x axis, the y axis and the z axis respectively in a σ coordinate system; T, S, P, ρ represent temperature, salinity, pressure and density, respectively; g is gravity acceleration; f is the Coriolis force parameter; K_m is the vertical eddy viscosity coefficient, K_h is the thermal vertical eddy viscosity diffusion coefficient; F_u and F_v represent the horizontal momentum diffusion terms; F_T, F_S are the horizontal temperature and salinity, respectively.

2.2. Model Configuration

Considering that there are many factors affecting the CDW (such as the Taiwan warm current) and in order to reduce the experimental error, the grid scope is large and the grid refined area includes the whole YRE. The model grid is shown in Figure 1. The calculation range of the model is 2436.7 km long and 1484.1 km wide from north to south, which is from 117° E to 137° E and 20° N to 40° N, including Chongming Island, Changxing Island and other major islands. The internal grids of the Yangtze River Estuary (YRE), especially those around the islands, the irregular boundaries and key research areas are more refined compared with the open sea grid. The model contains 12,583 nodes, 23,699 unstructured triangular elements and six sigma layers which are set in the vertical direction. The maximum resolution of the model is 25 km and the minimum resolution is 100 m. Data from ETOPO1, which is a 1 arc-minute global relief model of the Earth's surface that integrates land topography and ocean bathymetry released by the National Geophysical Data Center [18], are used for the offshore area of the model. The chart of China Navigation's assurance department is adopted to obtain the depth of the YRE and the shoreline is corrected by using Google Earth, while the large-scale and local water depths are shown in Figure 2.

In order to reduce the numerical calculation error, the trend of the open boundary should be basically vertical or parallel to the mainstream direction, insofar as possible. The tidal amplitudes of eight main tidal components (M_2, S_2, K_1, O_1, N_2, K_2, P_1 and Q_1) generated by the tidal fluctuation from the Tidal Model Driver [19] were used for the open boundary conditions. Considering the baroclinic effects caused by temperature and salinity, the initial temperature and salinity field of the model adopts the Hybrid Coordinated Ocean Model (HYCOM) data [20]; the meteorological input files such as heat flux, wind field forcing, evaporation and rainfall are reanalyzed by the Climate Forecast System Reanalysis (CFSR) [21] 6-hourly products provided by the National Center for Environmental Prediction (NCEP), which is widely used in meteorological and hydrological modeling [7,9,22]. The runoff of the YR adopts the monthly average discharge of the Xuliujing section in the *Water Resources Monitoring Bulletin of important control sections in the Yangtze River Basin*, issued by the Shanghai Water Conservancy Commission (SWCC) [23]. The internal and external mode separation calculation method of the FVCOM is used in the model, in which the external model time step is 1 s and the internal model time step is 10 s. The start-up mode of the model is a cold start and considering that it takes time for the model to be stable, the numerical simulation results were taken from 10 May to 30 November 2019. The calculations continue and the data are calculated by the model output every hour after a stable tidal wave is obtained.

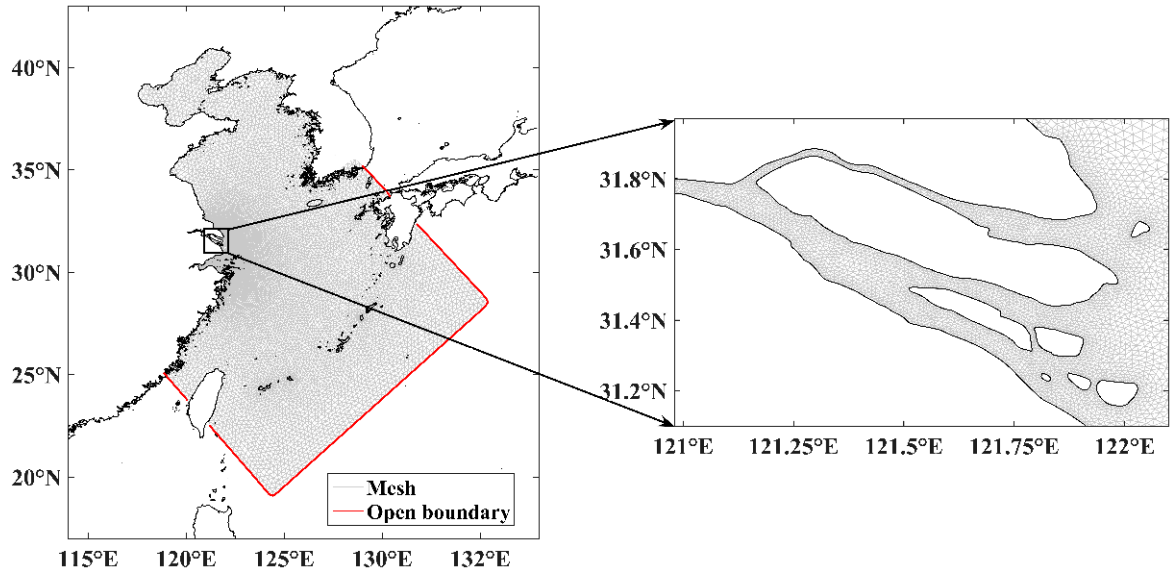


Figure 1. The computational domain and triangular mesh of the model.

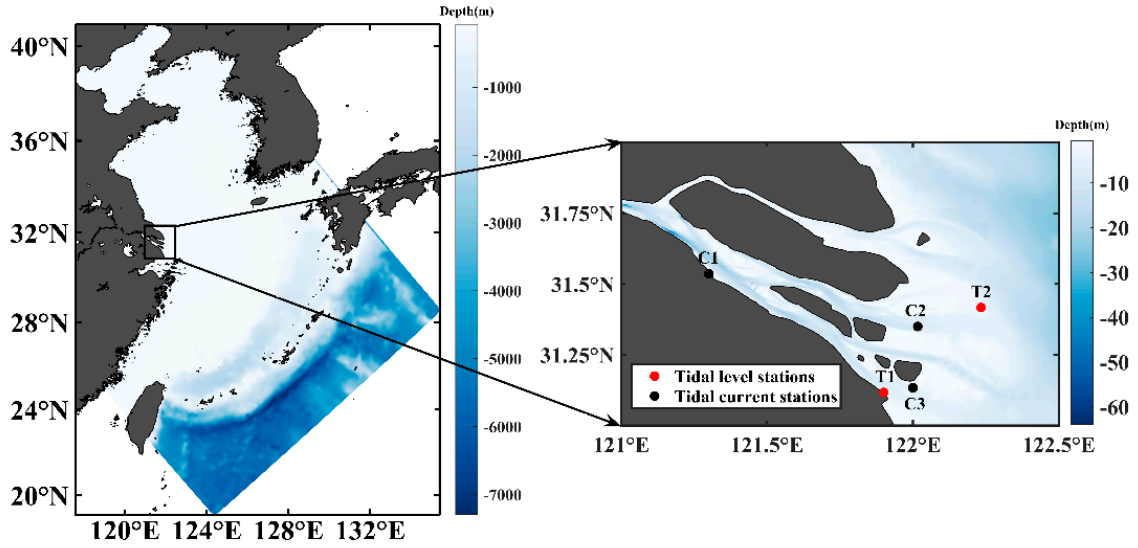


Figure 2. Model topography and local topography of the YRE and observation stations.

3. Results and Analysis

3.1. Model Validation

3.1.1. Validation of Tidal Level

Five observation stations were selected to verify the model according to the tide level and tidal current data released by the National Marine Data and Information Service (NMDIS) [24] in order to verify the accuracy. The tide level and the current station layout are shown in Figure 2. By comparing the observed data of the T1 and T2 stations with the simulated values of corresponding points, as shown in Figure 3, the simulation and observation of the two tide stations are in good agreement. The average errors of the T1 and T2 stations are 6.79 cm and 9.04 cm, respectively. The average error of amplitude of four principal components is 1.42 cm, and the average error of phase is 2.13° (Table 1). Therefore, the simulation results are in good agreement with the observation results.

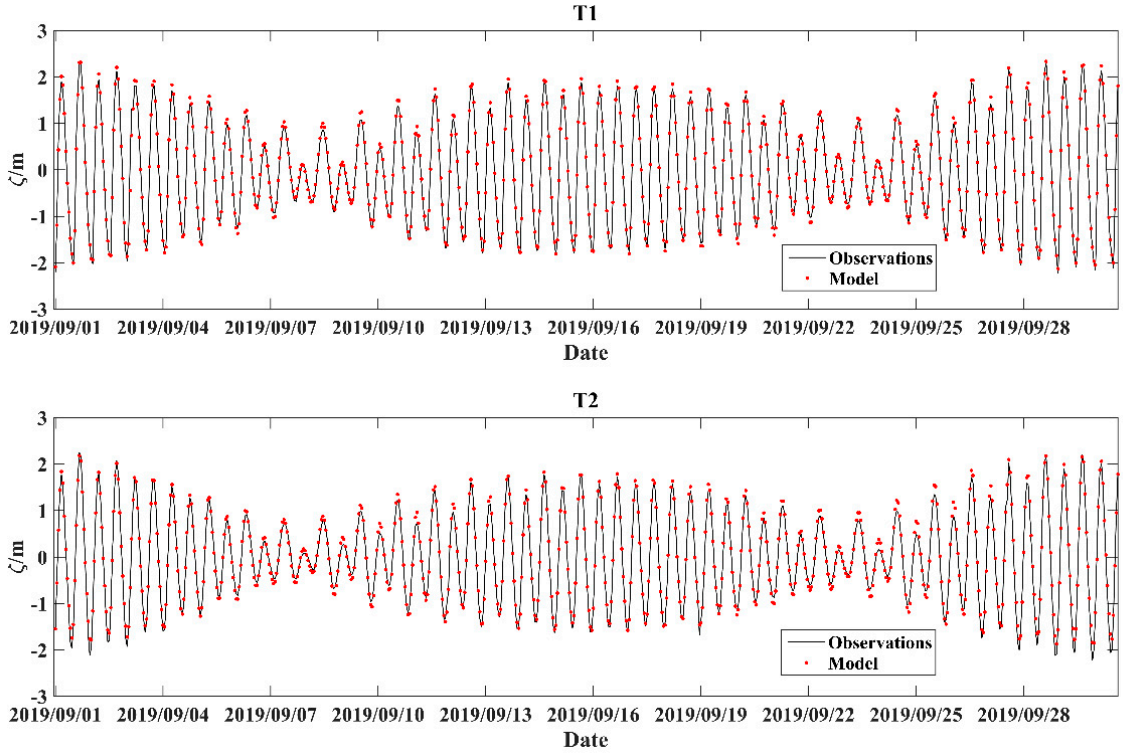


Figure 3. Comparison between calculated and observed tide elevation (T1: 121.9° E, 31.1° N. T2: 122.2° E, 31.4° N).

Table 1. Model-observation comparison of the main tidal constituents (O_1, K_1, M_2, S_2).

Constituents		T1			T2		
		Observation	Model	Error	Observation	Model	Error
O_1	Amplitude (cm)	19.26	18.70	−0.56	15.22	15.13	−0.09
	Phase (°)	28.48	35.39	6.91	0.56	0.69	0.13
K_1	Amplitude (cm)	22.23	25.10	2.87	20.34	21.81	1.47
	Phase (°)	67.81	71.12	3.31	55.20	53.87	−1.33
M_2	Amplitude (cm)	126.32	125.27	−1.05	111.44	110.99	−0.45
	Phase (°)	92.13	93.01	0.88	84.70	85.22	0.52
S_2	Amplitude (cm)	73.12	76.13	3.01	66.27	68.02	1.75
	Phase (°)	132.81	136.47	3.66	118.55	118.84	0.29

3.1.2. Validation of the Tidal Current

The calculation results of the tidal current at each station and the verification of the measured results are shown in Figures 4 and 5, respectively. The root-mean-square error of spring tide and neap tide velocity at each station is 16.18 cm/s, and the root-mean-square error of direction is less than 10% of the maximum flow direction. The direction of seawater movement in the open sea area is deflected by the influence of the deflection force of the Earth's rotation—the Coriolis force—while islands and the coast have the function of blocking and converging the offshore current and enhancing the influence of submarine friction. The output results of the model can only be selected in the triangle mesh closest to the observation point, which is difficult to keep the same position as the actual observation point. In addition, as the numerical treatment of large-scale water depth topography inevitably produces differences in local topography, resulting in errors between the calculation of tidal current and the measured fitting, it is considered that the hydrodynamic field of the model is well fitted.

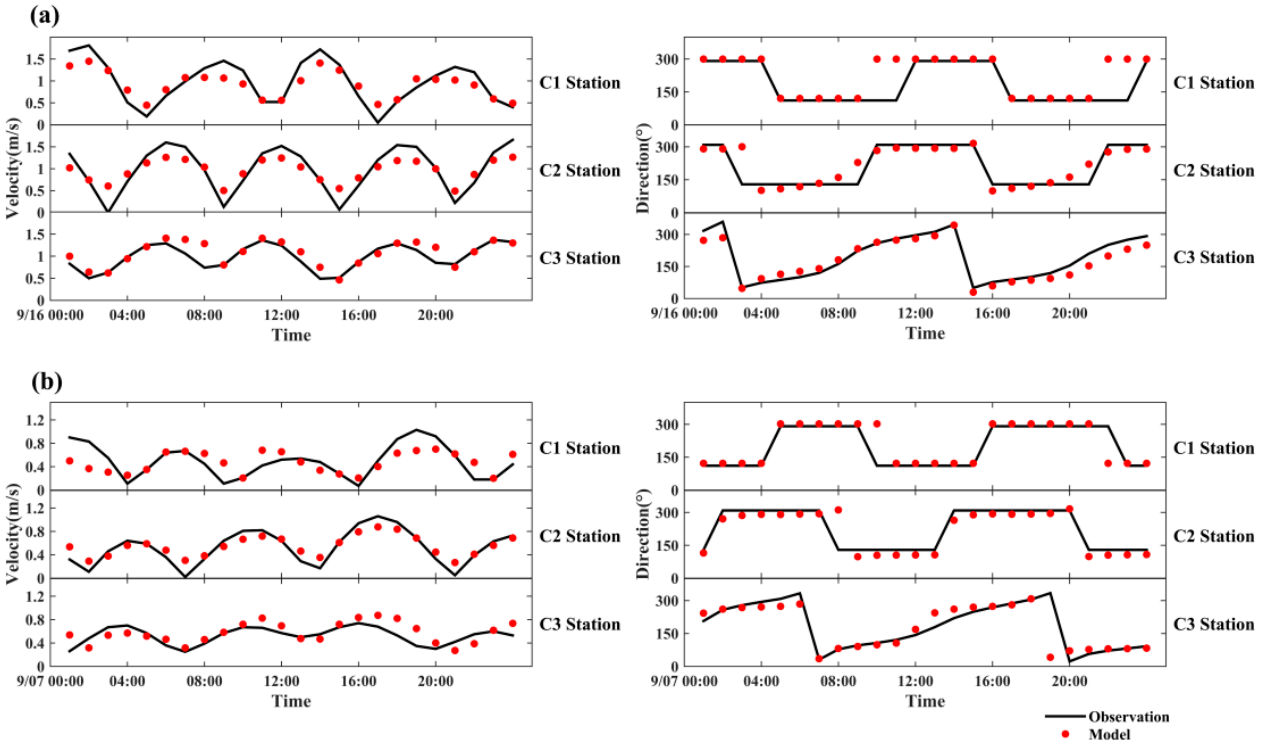


Figure 4. Tidal current validation of spring tide (**a**) and neap tide (**b**).

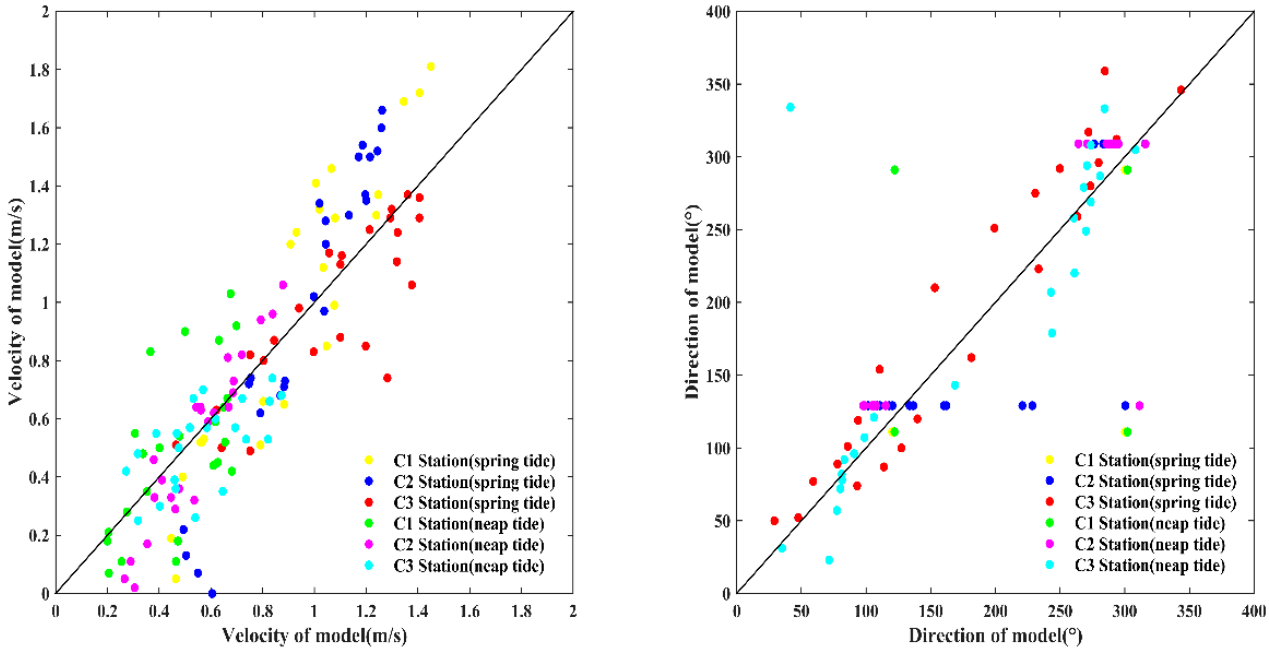


Figure 5. Matching of spring neap tide observations with model values. (The left figure shows the flow velocity fitting and the right figure shows the flow direction fitting).

3.1.3. Validation of Salinity

The salinity calculated with HYCOM data products [20] will be used for salinity verification of this model, and the comparison points are shown in Figure 6e,f. Figure 6 shows the comparison of salinity (b, d) calculated by the model with HYCOM (a, c) data products [20]. On 2 August, the CDW calculated by the model diffused eastward, which was basically the same as the CDW calculated by HYCOM data [20]. On 11 October, both

the CDW calculated by HYCOM data [20] and the CDW calculated by the model diffused southward. In addition, by comparing the surface salinity of the two stations (122° E, 31.9° N; 121.9° E, 29.2° N), the HYCOM data products [20] are highly correlated with the salinity calculated by the model, r = 0.95 (c) and r = 0.88 (f), respectively.

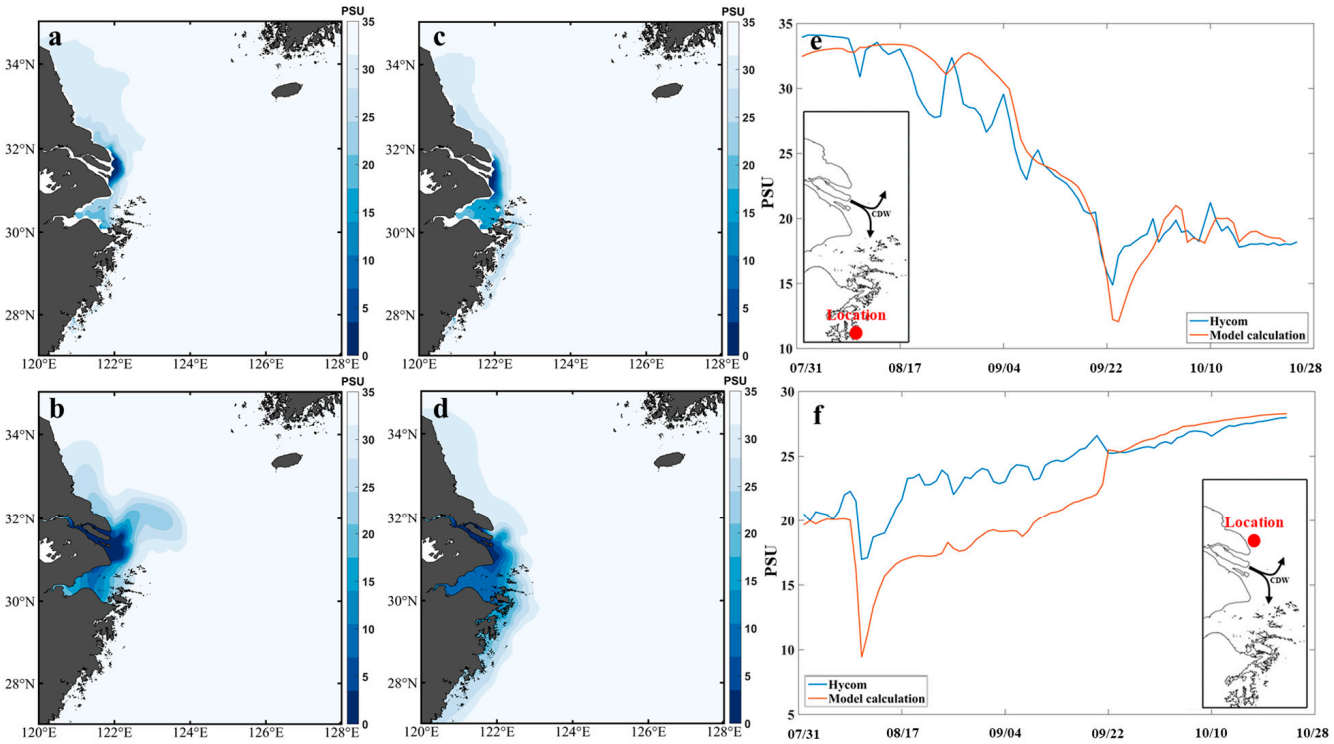


Figure 6. Comparison of model calculation and HYCOM data products ((**a**,**c**) are HYCOM data; (**b**,**d**) are model calculation results; (**e**,**f**) are the data comparison of the same position).

3.2. Characteristics of the Wind Field in the YRE

The YRE is located in the East Asian monsoon region, and the prevailing wind direction exhibits significant seasonal variation. Previous studies on the expansion of the CDW in summer were mostly related to the sea surface wind field [10,13,22]. Differences in wind direction and speed may have different effects on the expansion of fresh water, and it is therefore essential to study the characteristics of the wind field in the YRE. Figure 7 shows the frequency chart of wind direction and wind speed in the YRE (120° E to 124° E, 29° N to 33° N) for each month, obtained from the NCEP's CFSR reanalysis data. In terms of months, the main wind directions at the YRE from June to August in 2019 were southeast, south and east-northeast, respectively, and the frequency of the main wind direction was 15% in July 2019. The main wind directions from September to November were similar, and most of them were north-northeast or north due to the typhoon transit, while the maximum wind speed was larger in August and September 2019. In terms of the seasons, the average wind speed in autumn is stronger than that in summer, with wind from the east-southeast, south and east-northeast more common in summer, while those from the north-northeast and north are dominant in autumn.

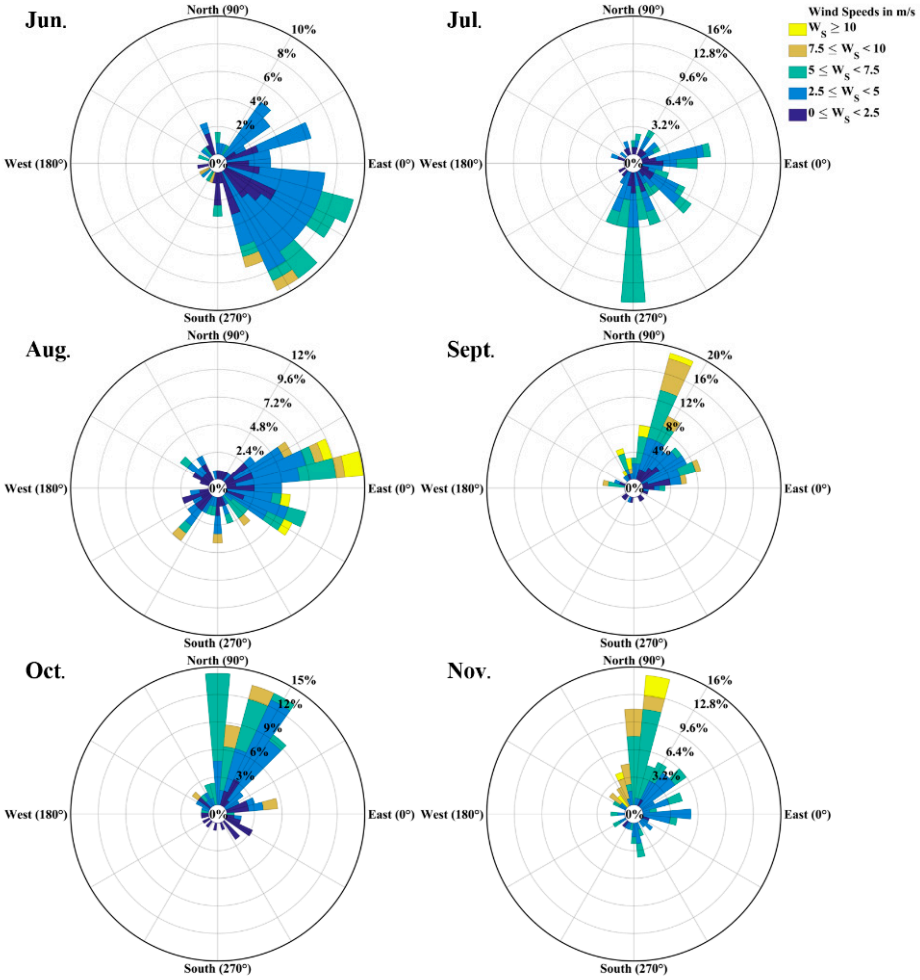


Figure 7. Wind rose of the YRE (120° E to 124° E, 29° N to 33° N) during June to November 2019. Length represents frequency and color represents speed.

3.3. Effect of Wind on the Path Turning of the CDW

The CDW is a water mass with a wide horizontal range and a thin thickness with characteristics of low salt, high oxygen, low transparency and turbidity. In order to suitably describe the expansion form of the CDW and referring to the previous definition of the CDW, the isohaline of 26‰ [3,8] is taken as the core area of the CDW and the expansion direction of the isohaline of 30‰ [7] is used to determine the maximum expansion scope in this paper. According to Figure 8, the core area of the CDW mainly extended to the northeast and northwest in the summer and to the southeast in the autumn of 2019. The CDW expands in a northwest direction with the action of the southeast wind in June. With an increase in the southeast wind and the runoff in the core area of fresh water, the core area of the CDW reaches 124° E in July and the low saltwater tongue extends obviously eastward. This is similar to the direction of the Ekman transport, that is, the CDW expands to the right of each wind direction [8]. In August, the wind direction near the YRE changes from southeast to east and the Ekman transport to the East is weakened, making the isohaline 30‰ closer to the shore, and the trend of the core area of the CDW near to the North Jiangsu coast. The core area of the CDW expanded to the South and contracted to the shore in September. This may be because typhoon Lingling (1913) and typhoon Tapah (1917) made a large amount of the CDW transport abnormally to the South. At the same time, the Ekman transport under the northeast wind had a westward component, which made the fresh water contract obviously to the West. In October and November, the expansion of the core area of the CDW is similar, and the core area of the CDW decreases

due to the month by month decrease in runoff. Under the action of a northerly wind, the 30‰ isohaline shrinks to the south, which is consistent with Guo et al.'s [6] conclusion. In order to better understand the expansion of the CDW over time, two areas were selected in the north and south of the YRE. Figure 9 shows that with the increase in runoff, the salinity of area A and area B gradually decreases. From July to August in 2019, area A is above 26, while area B is on the contrary. In September 2019, the salinity of area A decreased significantly, while that of area B continued to increase. This showed that the expansion direction of the CDW had changed.

In order to further study the effect of wind on the path turning of the CDW, this experiment simulated the diffusion of the CDW with an external wind field and windless conditions based on the FVCOM. Figure 10 clearly shows the difference in the expansion of the CDW in summer and autumn, with or without the wind field. After adding the wind field, the trend of the CDW moves upward, basically in the YRE, Hangzhou Bay, Zhoushan sea area, while the CDW without the wind field expands downward to 27° N in summer. The difference between July and August is the most obvious. The CDW with the wind field changes from the North Jiangsu coastal area to the Zhejiang coastal area, and the core area of the CDW does not exceed 32° N in autumn. The trend of the CDW without the wind field is basically the same, but extends to the North Jiangsu coast compared with the summer. Combined with the analysis of the wind field in this paper, Section 3.2, it was found that change of the wind field is consistent with the direction of the core area of the CDW. In terms of the difference of the residual current field ($\vec{V}_{Er} = \sum_{i=1}^{N} \vec{V}$) in the YRE when there is wind and when there is no wind, the direction of the surface residual current field is changed by the influence of the surface wind in summer and autumn, as shown in Figure 11. The residual current mainly flows to the east or northeast in summer and to the southeast in autumn. It can be seen that the surface wind can change the direction of the CDW by affecting the flow field in summer and autumn.

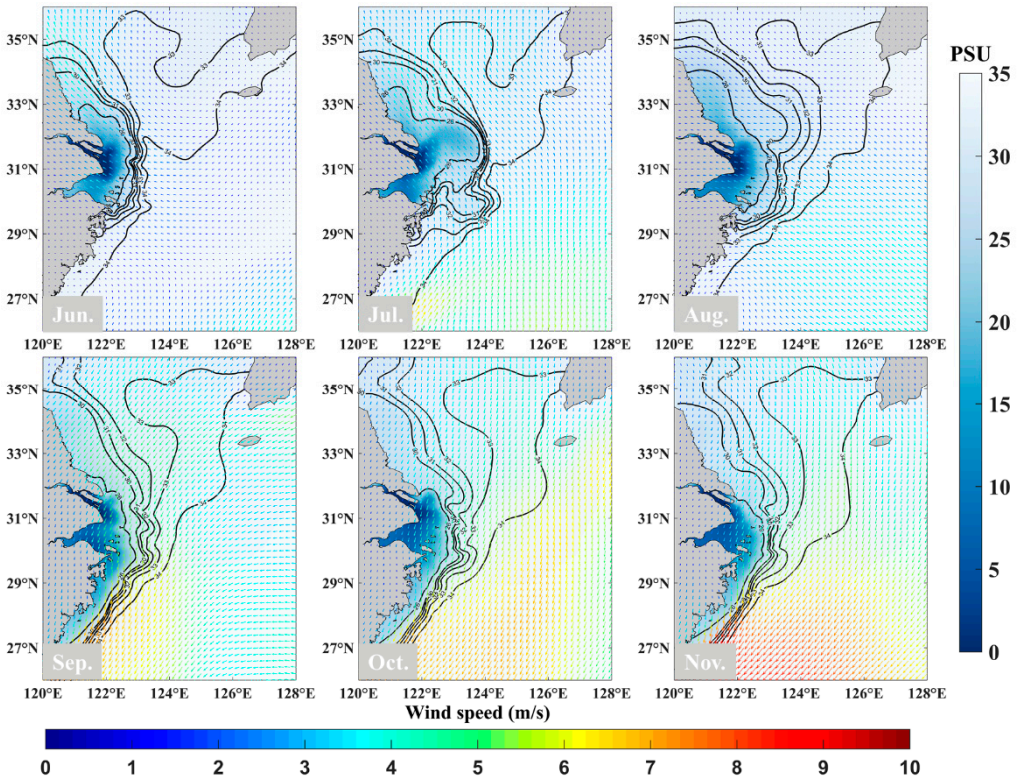


Figure 8. Monthly distribution of surface salinity in the YRE. The color represents the salinity (PSU), the arrow represents the monthly average wind field, the color represents the wind speed (m/s) and the black solid line represents the isohaline of 26‰, 30‰, 31‰, 32‰, 33‰ and 34‰, respectively.

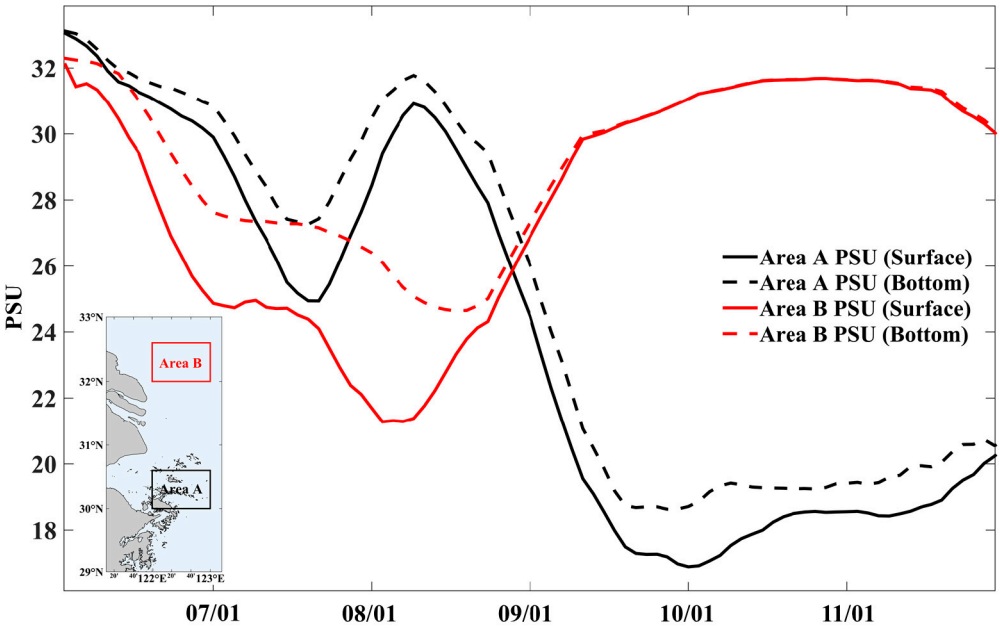


Figure 9. Salinity changes in the southern and northern Yangtze River Estuary.

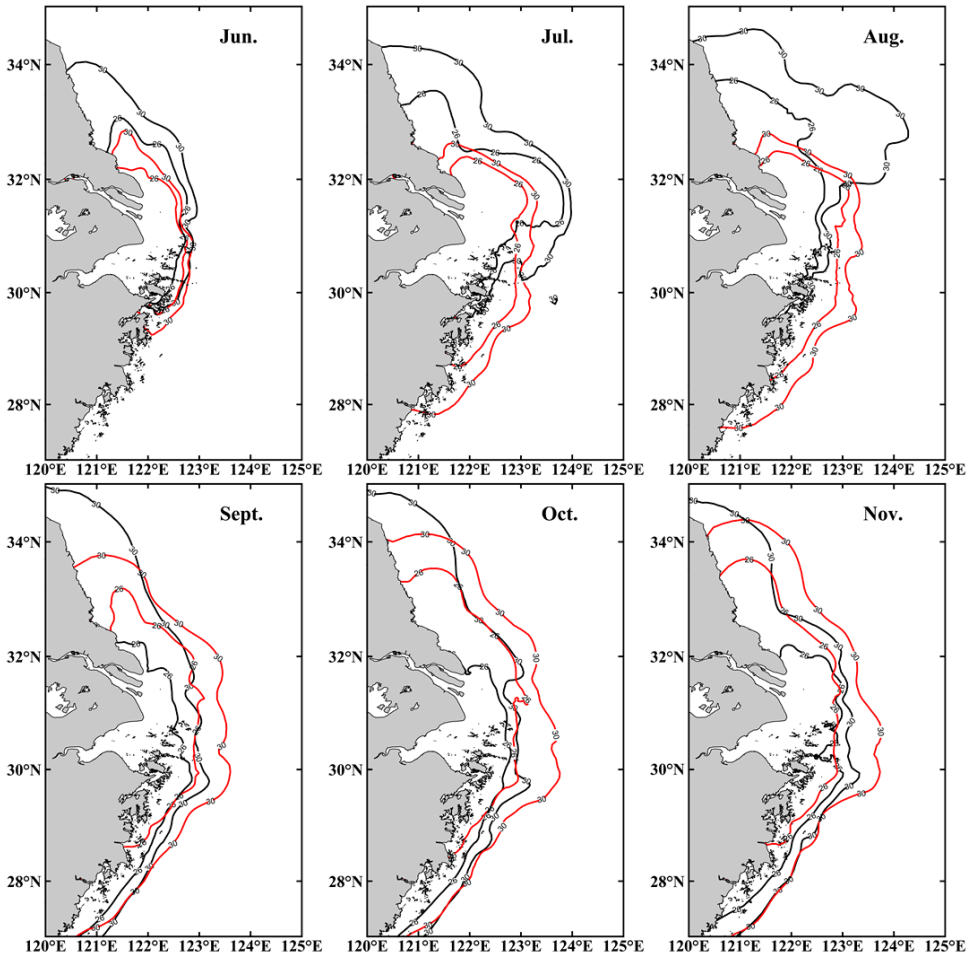


Figure 10. Distribution of surface salinity in the YRE with and without the wind field in summer and autumn. The black solid line and the red solid line represent the maximum expansion of the CDW with and without the wind field, respectively.

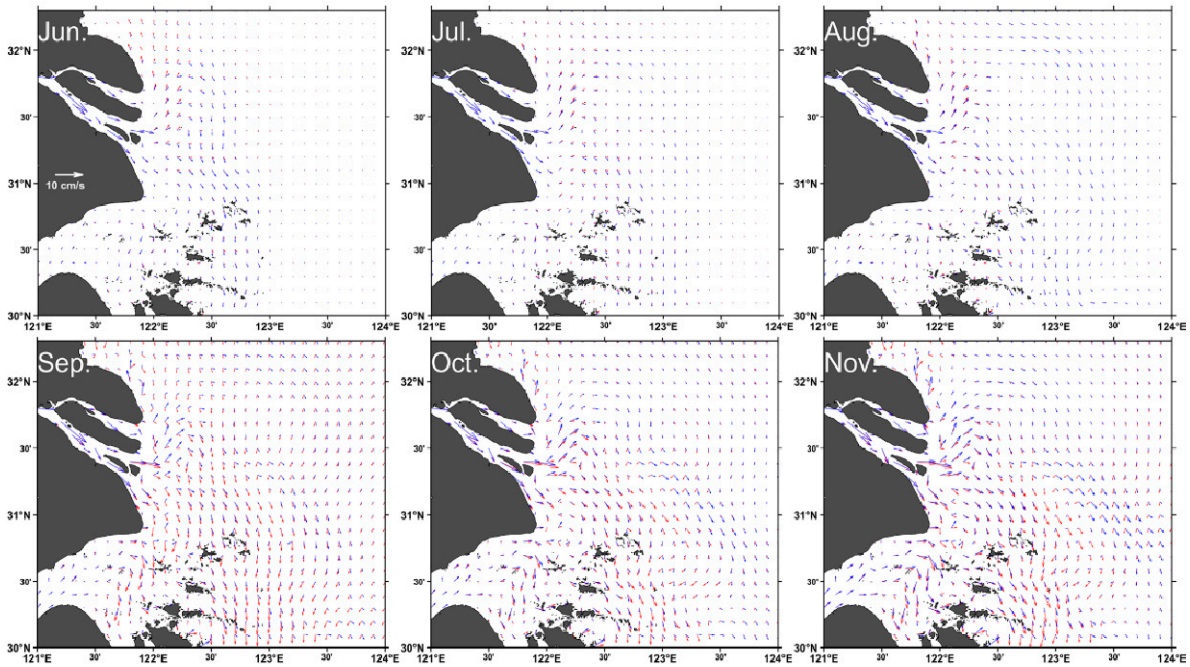


Figure 11. Surface residual current fields with and without the wind field in the YRE. The red and blue arrows indicate the residual current field with and without the wind field, respectively.

3.4. Influence of Typhoons on the Spreading Pattern of the CDW

Many previous studies have focused on the path turning and expansion of the CDW in single or multiple winds [8,25,26], with the CDW often affected by severe weather such as typhoons. Zhao et al. [5] found that the path turning of the CDW often occurs during the flood season. Typhoons landing in the East China Sea or in the eastern coastal areas of China usually occur from July to September [27], which represents the flood season of the YR. Typhoons transport a large amount of the CDW near the YRE to the open sea, accompanied by rainfall. Therefore, it is necessary to study the impact of typhoons on the CDW.

There were four typhoon events affecting the YRE from June to November 2019, along with typhoon Lekima (1909), typhoon Lingling (1913), typhoon Tapah (1917) and typhoon Mitag (1918) as shown in Figure 12, among which Lekima (1909) and Lingling (1913) were super typhoons. During the passage of a typhoon, the strong wind field will intensify the vertical mixing of sea water and increase the surface salinity [28]. Figure 13 shows the difference between the surface salinity and the bottom salinity before, during and after the typhoon transit. In order to better explain the impact of typhoon hedging on the expansion of the CDW, we selected two representative sites to explain the response time of the CDW to typhoons (Figure 14). The majority of the CDW left the YRE under the influence of a southeast wind caused by typhoon Lekima (1909) and approached the northwest coastal area, where the salinity of point A decreased rapidly (Figure 14). After the typhoon passed through, the CDW approached the North Jiangsu coast along with the main wind direction and the water tongue changed from northeast to northwest in August (Figure 8). Typhoons Lingling (1913), Tapah (1917) and Mitag (1918) all occurred in September, generating wind circles and vortices to the east of the YRE. The CDW was continuously transported to the Zhejiang coastal region under the influence of these typhoons with the same path and same wind direction, existing for a long period of time under the influence of the wind fields (Figure 14), resulting in the rapid downward expansion of the CDW in September (Figure 8). As shown in Figure 14, under the influence of typhoon Lekima (1909), the salinity of point A in the core area of the CDW rapidly decreased from 18 to 7 and returned to the original state after 25 days [27], the path turning of the CDW causing the sea water to

come close in and thereby increasing the salinity. It can be seen that typhoon Lekima (1909) caused the abnormal northward transport of the CDW. After the passage of the typhoon, the monsoon of that month kept the path of the CDW northward, but the abnormally transported CDW cannot exist for long, and even moved southward with the path of the CDW under the effect of the subsequent autumn monsoon (Figure 14). The salinity of point B changed under the influence of continuous typhoons, and the minimum salinity was 8 under the influence of typhoon Tapah (1917). Although the salinity gradually rose to 22, it decreased again under the influence of abnormal transportation of the CDW caused by typhoon Mitag (1918), and finally maintained a level between 17–19 due to the path turning downward of the CDW in autumn. Different from Lekima (1909), continuous typhoons cause a large amount of the CDW to be transported abnormally to the South and the monsoon of the current month also takes the CDW path to the south. However, continuous typhoons intermittently provide a large amount of the CDW and the CDW is continuously supplemented by the monsoon after the typhoon passes through (Figure 14). As a result, the abnormally transported flush water can exist for a long time.

In conclusion, typhoons make the CDW transport abnormally. In September 2019, following the passage of continuous typhoons, a large amount of flushing water was created with continuous abnormal transportation of the CDW and the expansion direction of the CDW also changed significantly.

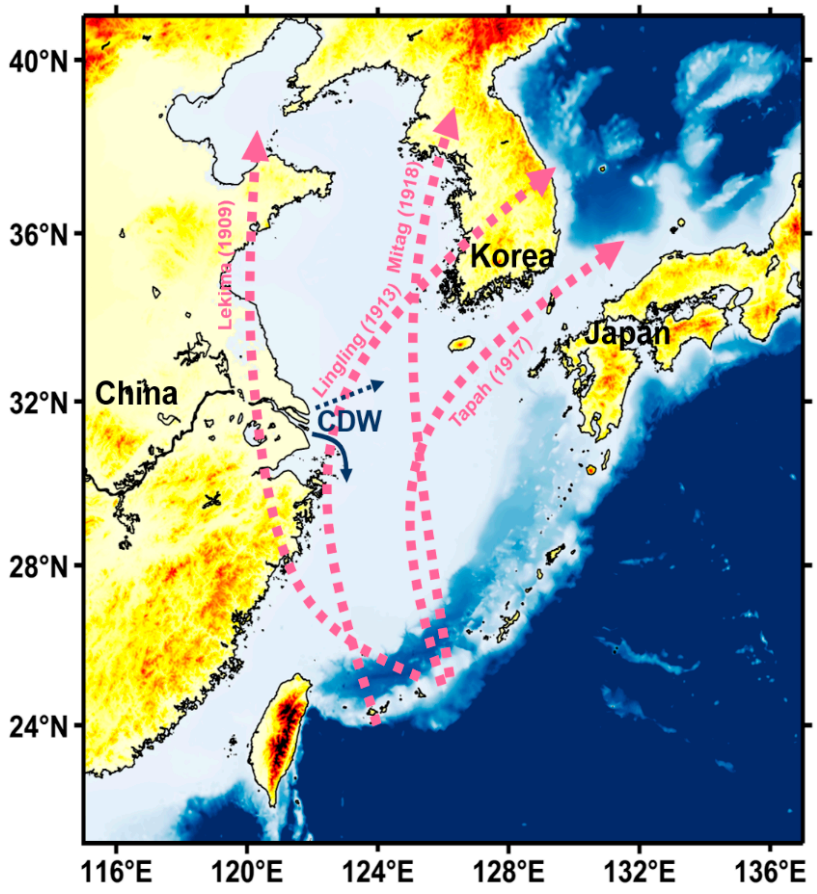


Figure 12. Typhoon track map affecting the YRE in 2019. The blue dotted arrow and the blue solid arrow indicate the direction of the CDW in summer and autumn, respectively, while the pink arrows represent typhoon Lekima (1909), typhoon Lingling (1913), typhoon Tapah (1917) and typhoon Mitag (1918), respectively.

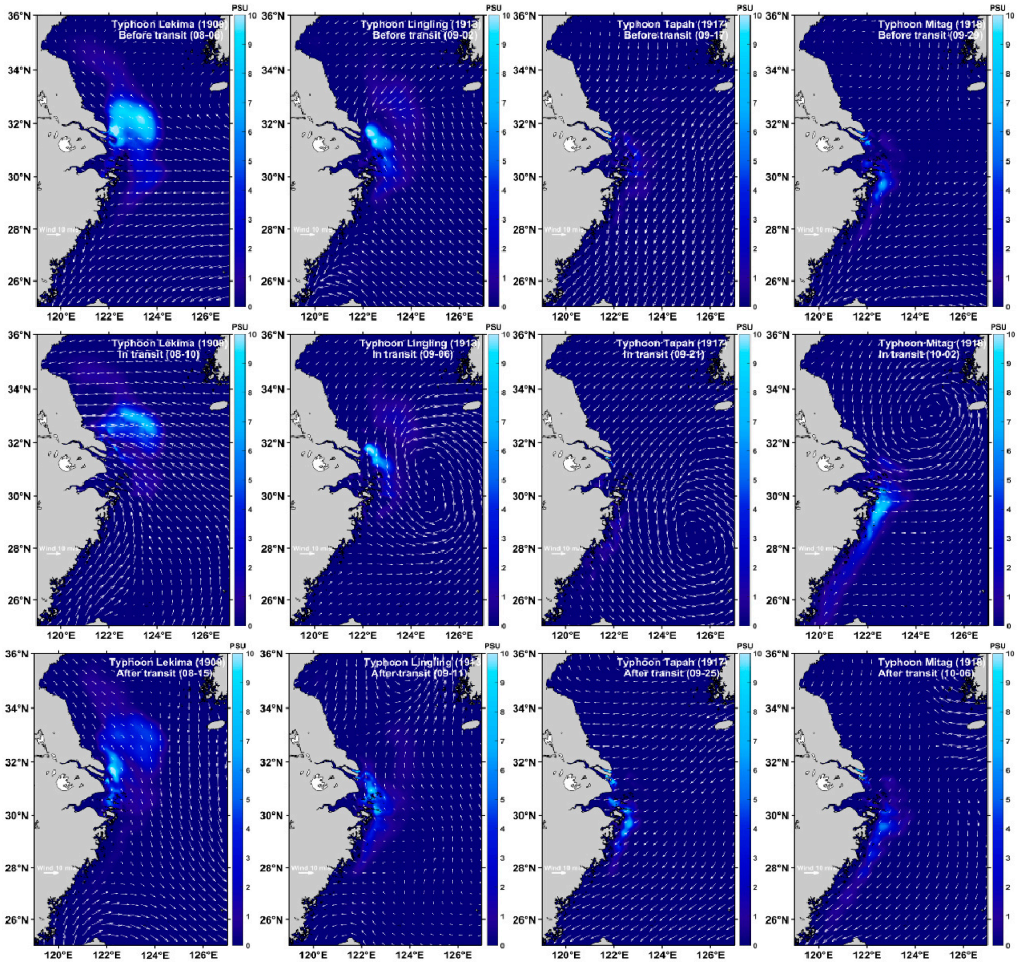


Figure 13. Effects of typhoons on the difference between surface salinity and bottom salinity of the CDW before, during and after typhoon transit. (The color is salinity difference, and the white arrow represents the wind field).

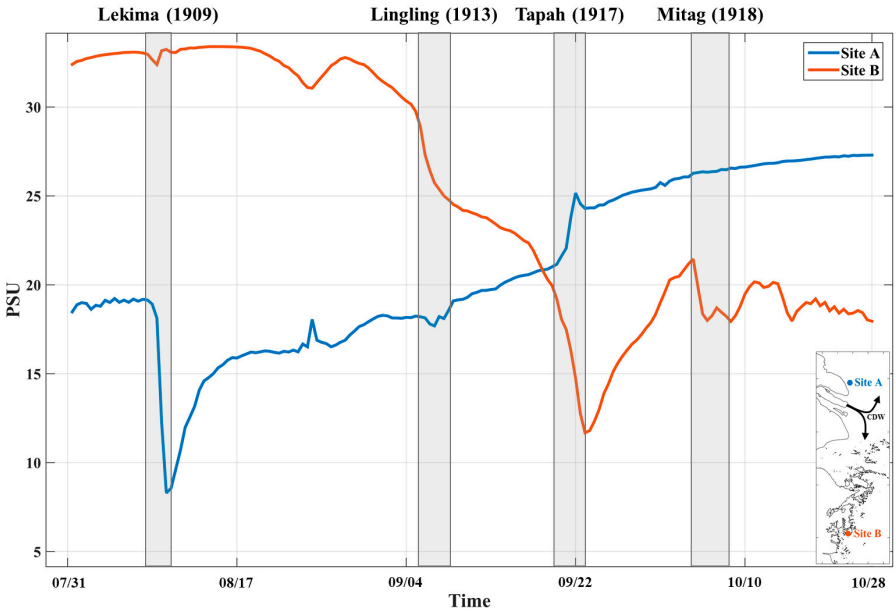


Figure 14. Salinity time series of points A and B. (The black arrow represents the different paths of the CDW in summer and autumn).

4. Conclusions

A three-dimensional hydrodynamic model for the YRE and its adjacent waters was established to study the expansion patterns of the CDW in summer and autumn. The main conclusions are as follows.

(1) In 2019, the CDW main expansion directions were northeast in summer and south in autumn, as per the monsoon. Seasonal variations of the wind field provide conditions for the CDW to expand in different forms.
(2) The influence of wind on the path turning of the CDW is obvious in contrast to the runoff. Wind leads to change of the residual current field, which causes the path turning of the CDW, while the runoff determines how far the core area extends.
(3) In the flood season of the YR in 2019, the frequent occurrence of typhoons accelerated change of the spreading form of the CDW. Continuous typhoons make transport a large amount of the CDW continuously and abnormally, which accelerates the path turning of the CDW.

This study focused on the impact of multiple factors on the distribution of the CDW, to facilitate understanding of the expansion and variation of the CDW in summer and autumn, and provides an important reference for predicting the expansion direction of the Yangtze River diluted water which is of great significance for further understanding the hydrological environment of the YRE.

Author Contributions: Conceptualization, J.Y. and W.H.; methodology, W.H.; software, W.H.; validation, W.H., M.B. and J.B.; formal analysis, W.H.; investigation, W.H.; resources, J.Y.; data curation, M.B.; writing—original draft preparation, M.B.; writing—review and editing, W.H.; visualization, W.H.; supervision, J.B.; project administration, J.B.; funding acquisition, J.Y. All authors have read and agreed to the published version of the manuscript.

Funding: The preparation of his work was supported by the National Key R&D Program of China [No.2018YFD0900805].

Institutional Review Board Statement: Not applicable.

Informed Consent Statement: Not applicable.

Data Availability Statement: Data sharing not applicable.

Conflicts of Interest: The authors declare no conflict of interest.

References

1. State Oceanic Administration. Bulletin of China Marine Environmental Status [EB/OL]. Available online: http://www.mee.gov.cn/hjzl/sthjzk/jagb/ (accessed on 1 December 2019).
2. Guo, Y.; Yang, Z. The ecological studies on the phytoplankton over the continental shelf of the East China Sea in the summer of 1976. *J. Mar. Sci.* **1982**, *19*, 11–32.
3. Wang, G.; Huang, X.; Jiang, X.; Hong, J. The distribution and characteristics of Skeletonema costatum red tides occurred Changjiang Estuary. *Mar. Sci.* **1993**, *3*, 51–55.
4. Gu, Y. A study on the cause of the path turning of the Changjiang River Diluted Water. *Oceanol. Limnol. Sin.* **1985**, *16*, 354–363.
5. Zhao, B. On the turning mechanism of the Yangtze River diluted water. *Acta Oceanol. Sin.* **1991**, *5*, 600–610.
6. Le, K. A preliminary study of the path of the Changjiang Diluted Water. *Oceanol. Limnol. Sin.* **1984**, *2*, 157–167.
7. Guo, Y.; Rong, Z.; Chi, Y.; Li, X.; Na, R. The modeling study of interannual variability of Changjiang River plume in summer season. *Oceanol. Limnol.* **2020**, *4*, 30–41.
8. Liu, B.; Li, J.; Feng, L. A modeling study of the effect of wind on Changjiang (Yangtze) River Diluted Water in summer. *Acta Oceanol. Sin.* **2013**, *35*, 25–37.
9. Wang, K.; Xiong, X.; Guo, B.; Hua, F.; Jiang, Z. The extension form and seasonal variation of the Changjiang Diluted Water during 2006–2007. *Coast. Eng.* **2012**, *1*, 46–54. [CrossRef]
10. Zhou, F.; Xuan, J.; Ni, X.; Huang, D. A preliminary study on variations of the Changjiang Diluted Water between August 1999 and 2006. *Acta Oceanl. Sin.* **2009**, *4*, 1–12.
11. Pan, Y.; Huang, S. Analysis on the path of transportation and diffusion of Changjiang diluted water. *Donghai Mar. Sci.* **1997**, *2*, 26–30.
12. Pu, Y. The summer salinity distribution types of the 30° N profile in the East China Sea. *Donghai Mar. Sci.* **2002**, *20*, 1–13.

13. Wang, J.; Wang, Y.; Wang, G. Analysis of direction change mechanism of the Changjiang River diluted water based on FVCOM and observation. *Adv. Earth Sci.* **2012**, *27*, 194–201.
14. Chen, C.; Liu, H.; Beardsley, R. An unstructured grid, finite volume, three-dimensional, primitive equation ocean model: Application to coastal ocean and estuaries. *J. Atmos. Ocean. Technol.* **2003**, *20*, 159–186. [CrossRef]
15. Chen, C.; Beardsley, R.; Cowles, G. An unstructured grid, finite-volume coastal ocean model (FVCOM) system. *Oceanography* **2006**, *19*, 78–89. [CrossRef]
16. Yu, H.; Wang, Z.; Kuang, L.; Wang, L.; Bao, X.; Wu, H.; Wang, X.; Deng, X. A numerical study on the circulation and tide in a zigzag bay. *Acta Oceanol. Sin.* **2015**, *1*, 119–128. [CrossRef]
17. Qu, D.; Yu, H.; Sun, Y.; Zhao, Y.; Wei, Q.; Yu, H.; Kelly, M.; Yuan, Y. Numerical study on the summertime patches of red tide in the adjacent sea of the Changjiang (Yangtze) River Estuary, China. *Mar. Pollut. Bull.* **2019**, *143*, 242–255. [CrossRef]
18. National Geophysical Data Center. ETOPO1 Global Relief Model [DB/OL]. Available online: http://www.ngdc.noaa.gov/mgg/global/ (accessed on 1 September 2019).
19. Padman, L.; Erofeeva, S. *Tide Model Driver (TMD) Manual*; Earth & Space Research: Seattle WA, USA, 2005.
20. Asia-Pacific Data-Research Center. HYCOM Global Daily Snapshot 0Z 1/12 Degree GOFS 3.1 Analysis (GLBv0.08) [DB/OL]. Available online: http://apdrc.soest.hawaii.edu/las/v6/dataset?catitem=11493 (accessed on 1 June 2020).
21. Saha, S.; Moorthi, S.; Pan, H.; Wu, X.; Wang, J.; Nadiga, S.; Tripp, P.; Kistler, R.; Woollen, J.; Behringer, D.; et al. The NCEP Climate Forecast System Reanalysis. *B Am. Meteorol. Soc.* **2010**, *91*, 1015–1058. [CrossRef]
22. Tao, L.; Sun, J.; Liu, H.; Li, Y.; Shang, J.; Lin, B.; Nie, Z.; Yuan, D. Study on water exchange in Bohai Bay under effects of tides and seasonal winds. *J. Hydrol. Eng.* **2020**, *39*, 99–107.
23. Shanghai Water Conservancy Commission. Water Resources Monitoring Bulletin of Important Control Sections in the Yangtze River Basin [EB/OL]. Available online: http://www.cjw.gov.cn/ (accessed on 1 June 2020).
24. National Marine Data and Information Service [DB/OL]. Available online: http://global-tide.nmdis.org.cn/ (accessed on 1 August 2020).
25. Li, B.; Lu, J.; Wang, P.; Wang, K. Isolated Low-Salinity Water mass in expansion area of Changjiang Diluted Water. *Oceanol. Limnol. Sin.* **2019**, *6*, 1181–1190.
26. Chen, C.; Xue, P.; Ding, P.; Beardsley, R.C.; Xu, Q.; Mao, X.; Gao, G.; Qi, J.; Li, C.; Lin, H.; et al. Physical mechanisms for the offshore detachment of the Changjiang Diluted Water in the East China Sea. *J. Geophys. Res.* **2008**, *113*, C02002.
27. Zhang, Z. *Dynamical Response of Changjiang River Plume Extension to Typhoon Events*; East China Normal University: Shanghai, China, 2020.
28. Blair, A.; Ginis, I.; Hara, T.; Ulhorn, E. Impact of langmuir turbulence on upper ocean response to hurricane edouard: Model and observations. *J. Geophys. Res.* **2017**, *122*, 9712–9724. [CrossRef]